JOURNAL OF CHEMICAL INFORMATION AND MODELING

Article

pubs.acs.org/jcim

Thermodynamic Characterization of New Positive Allosteric Modulators Binding to the Glutamate Receptor A2 Ligand-Binding Domain: Combining Experimental and Computational Methods Unravels Differences in Driving Forces

Ann-Beth Nørholm,[†,‡] Pierre Francotte,[§] Eric Goffin,[§] Iuliana Botez,[∥] Laurence Danober,[⊥] Pierre Lestage,[⊥] Bernard Pirotte,[§] Jette S. Kastrup,[†] Lars Olsen,[†] and Chris Oostenbrink*[,‡]

[†]Department of Drug Design and Pharmacology, Faculty of Health and Medical Sciences, University of Copenhagen, Universitetsparken 2, DK-2100 Copenhagen, Denmark

[‡]Institute of Molecular Modeling and Simulation, University of Natural Resources and Life Sciences, Muthgasse 18, A-1190 Vienna, Austria

[§]Department of Medicinal Chemistry, Center for Interdisciplinary Research on Medicines (CIRM), University of Liege, Avenue de l'Hôpital, 1, B36, B-4000 Liège, Belgium

[∥]Pôle d'Expertise Chimie-Chimie Médicinale, Institut de Recherches Servier, 129 Chemin de Ronde, F-78290 Croissy-sur-Seine, France

[⊥]Pôle d'Innovation Thérapeutique en Neuropsychiatrie, Institut de Recherches Servier, 129 Chemin de Ronde, F-78290 Croissy-sur-Seine, France

Supporting Information

ABSTRACT: Positive allosteric modulation of the ionotropic glutamate receptor GluA2 presents a potential treatment of cognitive disorders, for example, Alzheimer's disease. In the present study, we describe the synthesis, pharmacology, and thermodynamic studies of a series of monofluoro-substituted 3,4-dihydro-2*H*-1,2,4-benzothiadiazine 1,1-dioxides. Measurements of ligand binding by isothermal titration calorimetry (ITC) showed similar binding affinities for the modulator series at the GluA2 LBD but differences in the thermodynamic driving forces. Binding of **5c** (7-F) and **6** (no-F) is enthalpy driven, and **5a** (5-F) and **5b** (6-F) are entropy driven. For **5d** (8-F), both quantities were equal in size. Thermodynamic integration (TI) and one-step perturbation (OSP) were used to calculate the relative binding affinity of the modulators. The OSP calculations had a higher predictive power than those from TI, and combined with the shorter total simulation time, we found the OSP method to be more effective for this setup. Furthermore, from the molecular dynamics simulations, we extracted the enthalpies and entropies, and along with the ITC data, this suggested that the differences in binding free energies are largely explained by the direct ligand-surrounding enthalpies. Furthermore, we used the OSP setup to predict binding affinities for a series of polysubstituted fluorine compounds and monosubstituted methyl compounds and used these predictions to characterize the modulator binding pocket for this scaffold of positive allosteric modulators.

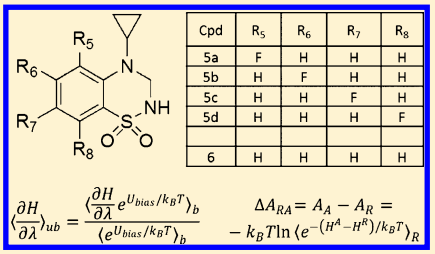

Cpd	R_5	R_6	R_7	R_8
5a	F	H	H	H
5b	H	F	H	H
5c	H	H	F	H
5d	H	H	H	F
6	H	H	H	H

$$\left\langle \frac{\partial H}{\partial \lambda} \right\rangle_{ub} = \frac{\left\langle \frac{\partial H}{\partial \lambda} e^{U_{bias}/k_B T} \right\rangle_b}{\left\langle e^{U_{bias}/k_B T} \right\rangle_b} \qquad \Delta A_{RA} = A_A - A_R = -k_B T \ln \left\langle e^{-(H^A - H^R)/k_B T} \right\rangle_R$$

INTRODUCTION

The α-amino-3-hydroxy-5-methylisoxazole-4-propionic acid (AMPA) receptors mediate influx of metal ions across post-synaptic membranes in the mammalian central nervous system (CNS) in response to the neurotransmitter glutamate.[1] AMPA receptors form homotetrameric and heterotetrameric ion channels; each subunit consists of a N-terminal domain (NTD), a ligand-binding domain (LBD), a membrane-spanning region, and an intracellular C-terminal domain. In the full-length homotetrameric glutamate receptor A2 (GluA2), the LBD subunits are arranged as a dimer of dimers.[2] The endogenous ligand (*S*)-glutamate binds in the agonist binding site, whereas positive allosteric modulators have been shown to bind at the dimer interface (Figure 1A–C). Upon (*S*)-glutamate binding, the LBD closes like a clamshell, which leads to a structural rearrangement and opening of the ion channel.[3] The receptor may undergo desensitization, triggered by a rearrangement of the LBD dimer where (*S*)-glutamate is still bound but the ion channel is closed.[1] Positive allosteric modulators potentiate the effect of (*S*)-glutamate by either stabilizing the (*S*)-glutamate bound conformation and thus slowing deactivation or by stabilizing the subunit interface, postponing the interface rearrangement and subsequent closure of the ion channel with (*S*)-glutamate bound and hence slowing desensitization.[4,5] This fine-tuning of receptor signaling represents a promising therapeutic strategy in the treatment of several neurological diseases such as Alzheimer's disease,

Received: September 13, 2014
Published: November 24, 2014

dx.doi.org/10.1021/ci500559b | *J. Chem. Inf. Model.* 2014, 54, 3404–3416

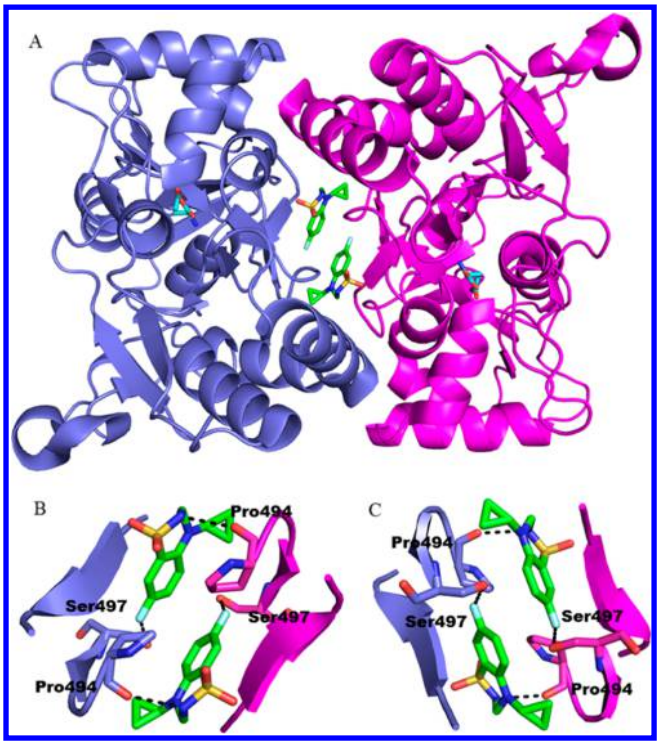

Figure 1. Cartoon representation of the previously reported structure of GluA2−LBD−L483Y−N754S in complex with glutamate and **5c**. (A) Each LBD monomer (blue and magenta) adopts a clamshell-like form around the endogenous ligand glutamate (shown in cyan stick representation). The positive allosteric modulator binding pocket lies in the LBD dimer interface where two copies of the positive allosteric modulator **5c** (shown in green stick representation) bind. (B and C) Zoom on the positive allosteric modulator binding pocket. C is rotated 180° relative to B. Dashed lines indicate potential hydrogen bonds (**5c** to Pro494) or hydrogen−fluorine bonds (**5c** to Ser497). The figure was prepared using PyMOL (PyMOL Molecular Graphics System, version 1.5.0.5, Schrödinger, LLC) and structure coordinates from the Protein Data Bank (PDB code 4N07).

schizophrenia, and attention deficit hyperactivity disorder (ADHD).

In recent years, significant improvements in the thermodynamic characterization of small-molecule inhibitor complexes with receptors and enzymes have been made, both by experimental as well as by computational means. Currently, the main experimental approach is isothermal titration calorimetry (ITC),[6] while computationally, the necessary simulation time has become accessible to compute free-energy differences from statistical mechanical approaches.[7] Whereas successful calculations of binding free energies are now more common,[8] calculation of the individual enthalpic and entropic contributions remains more challenging.[9] Furthermore, difficulties in drug design arise from enthalpy−entropy compensation,[10,11] a thermodynamic concept where changes in the entropic contribution are counteracted by changes in the enthalpic contribution and *vice versa*. Moreover, it was shown that binding affinity is correlated to neither enthalpy nor entropy alone.[12] For using computational methods in drug development, it is important to understand how the individual interactions in the protein−ligand system contribute to the enthalpy−entropy compensation. It has been shown that the energetic contributions from the solvent reorganization exactly cancel,[13−15] and therefore, the calculation of the direct ligand-surrounding contributions rather than the contributions of the interactions of the surroundings with itself can lead to additional insight. The contribution of the interactions of the surroundings with itself is also included in the experimentally determined data from ITC, and thus, the combined use of experimental and computational methods allows for a more thorough decomposition of the energetic contributions, where the ligand-surrounding energy terms are analyzed. This provides a more detailed analysis of the energetic contributions that contribute directly to ligand binding, which would not be possible using experimental methods alone.

In the present study, we report the synthesis and pharmacological characterization of three new positive allosteric modulators, where the substitution pattern of fluorine on the benzene nucleus of 3,4-dihydro-2*H*-1,2,4-benzothiadiazine 1,1-dioxide (BTD) is varied. These modulators are derived from the previously described 4-cyclopropyl-7-fluoro-3,4-dihydro-2*H*-1,2,4-benzothiadiazine 1,1-dioxide (**5c**)[16] (Figure 2). We

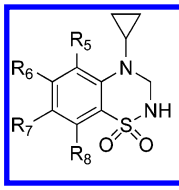

Cpd	R_5	R_6	R_7	R_8
5a	F	H	H	H
5b	H	F	H	H
5c	H	H	F	H
5d	H	H	H	F
6	H	H	H	H

Figure 2. Chemical structure of the 4-cyclopropyl-3,4-dihydro-2H-1,2,4-benzothiadiazine 1,1-dioxides (BTDs) studied. All compounds differ only by the substitution pattern at positions **5**, **6**, 7, or **8**.

characterized the thermodynamics of binding to the dimeric GluA2 LBD of this modulator series using ITC. To complement the experimentally determined thermodynamic details of binding, we used both thermodynamic integration (TI) and one-step perturbation (OSP) to set up a method to calculate the relative free energy of binding. TI is a highly accurate method to estimate free-energy differences between compounds, but it also has a high computational expense.[17] The OSP method takes advantage of using a single reference molecule that is representative of several compounds of interest and thus significantly improves the efficiency.[18] From these simulations, we extracted the reduced enthalpies and entropies to perform a detailed analysis of the direct enthalpy−entropy contributions to ligand binding. Finally, we used the OSP data to make predictions of new compounds covered by the reference molecule, allowing for a detailed QSAR analysis of the modulator binding pocket. To our best knowledge, the present work represents the first free energy calculations of GluA2 LBD positive allosteric modulators.

MATERIALS AND METHODS

Chemistry. All commercial chemicals (Sigma-Aldrich, Belgium; Appolo Scientific, United Kingdom; and Fluorochem, United Kingdom) and solvents were reagent grade and used without further purification. Melting points were determined on a Stuart SMP3 apparatus in open capillary tubes and are uncorrected. NMR spectra were recorded on a Bruker Avance 500 spectrometer (^{1}H, 500 MHz; ^{13}C, 125 MHz) using DMSO-d_6 as solvent and tetramethylsilane (TMS) as internal standard; chemical shifts are reported in δ values (ppm) relative to internal TMS. Elemental analyses (C, H, N, S) were carried out on a Thermo Flash EA 1112 series elemental analyzer and were within ±0.4% of the theoretical values. This analytical

dx.doi.org/10.1021/ci500559b | J. Chem. Inf. Model. 2014, 54, 3404−3416

method certified a purity of ≥95% for each tested compound. All reactions were followed by TLC (silica gel 60F_{254} Merck), and visualization was accomplished with UV light (254 or 366 nm). The synthesis of **5c** starting from 2,5-difluorobenzenesulfonamide (**2c**) has been previously described.[16] Synthesis of the other compounds was performed according to the scheme in Figure 3.

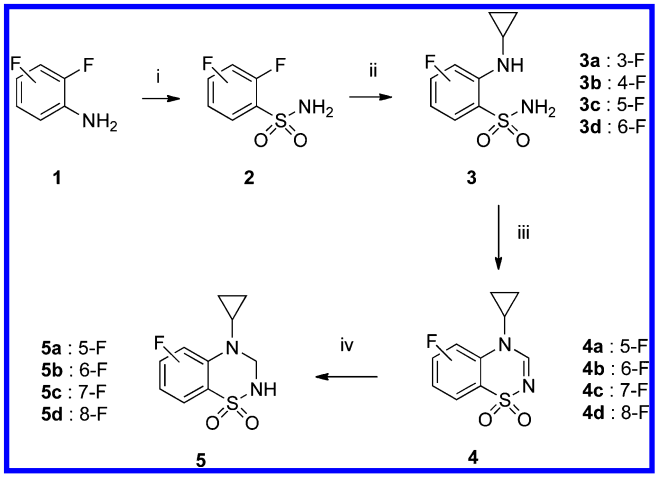

Figure 3. Schematic representation of the synthesis of compounds **5a**, **5b**, **5c**, and **5d**. Reagents: (i) 1. HNO_2, −5 °C; 2. SO_2, Cu_2Cl_2, 15 min; 3. NH_3 (60−70%); (ii) cyclopropylamine, dioxane, 100−110 °C, 24 h (80−90%); (iii) $HC(OEt)_3$, 130−150 °C, 24−48 h (70−80%); and (iv) $NaBH_4$, isopropanol, 50−55 °C, 5−10 min. (80−85%).

General Procedure for the Synthesis of Fluoro-Substituted 2-Fluorobenzenesulfonamides (2). Glacial acetic acid (30 mL) introduced in a round-bottomed flask (500 mL) was saturated for 30 min with gaseous sulfur dioxide. An aqueous solution of cupric chloride (1.5 g in 10 mL) was added to this solution giving a suspension of cuprous chloride (suspension A). In another flask, the appropriate fluoro-substituted 2-fluoroaniline (**1**; 5 g) was dissolved in a mixture of glacial acetic acid (30 mL) and 12 N HCl (15 mL), and the resulting solution (solution B) was cooled in an ice/salt bath (−5 °C). A solution of sodium nitrite (2.5 g) in water (10 mL) was added dropwise to solution B, and the resulting mixture was slowly added to suspension A and stirred in an ice bath for 15 min. The reaction mixture was then poured in water (200 mL) and diethyl ether (200 mL). The organic layer was separated, washed with water (100 mL), and concentrated to dryness under reduced pressure. The residue of the fluoro-substituted 2-fluorobenzenesulfonyl chloride was dissolved in dioxane (25 mL), and this solution was poured under stirring onto a cooled mixture of concentrated ammonia (25 mL) and water (10 mL). After 30 min, the reaction mixture was concentrated under reduced pressure, and the resulting precipitate of the final compound was collected by filtration, washed with water, and purified by crystallization in methanol−water (yield: 60−70%). 2,6-Difluorobenzenesulfonamide (**2d**) was used from a commercial source (Fluorochem, ref 017310).

General Procedure for Synthesis of Fluoro-Substituted 2-Cyclopropylaminobenzene-sulfonamides (3). A solution of the appropriate fluoro-substituted 2-fluorobenzene-sulfonamide (**2**) (3 g) in dioxane (30 mL) and cyclopropyl-amine (3 mL) was heated in a closed vessel at 100−110 °C for 24 h. The solvent and excess of amine were removed by distillation under reduced pressure, and the residue was dissolved in methanol (20 mL). The methanolic solution was cooled and mixed with water (60 mL) under stirring. The resulting precipitate was collected by filtration, washed with water, dried, and used in the next step without further purification (yield: 80−90%).

General Procedure for Synthesis of Fluoro-Substituted 4-Cyclopropyl-4*H*-1,2,4-benzothiadiazine 1,1-Dioxides (4). In an open vessel, a mixture of the appropriate fluoro-substituted 2-cyclopropylaminobenzenesulfonamide (**3**) (2 g) and triethyl orthoformate (20 mL) was heated at 130−150 °C for 24−48 h. The resulting suspension was cooled in an ice bath, and the insoluble material was collected by filtration, washed with diethyl ether, dried, and crystallized in methanol (yield: 70−80%).

General Procedure for Synthesis of Fluoro-Substituted 4-Cyclopropyl-3,4-dihydro-2*H*-1,2,4-benzothiadiazine 1,1-Dioxide (5). A mixture of the appropriate fluoro-substituted 4-cyclopropyl-4*H*-1,2,4-benzothiadiazine 1,1-dioxide (**4**) (1.9 g) and isopropanol (50 mL) was supplemented with finely divided sodium borohydride (1 g) and then heated at 50−55 °C for 5−10 min. The solvent was removed by distillation under reduced pressure, and the residue was taken up with water (50 mL). The resulting suspension was slightly acidified by the addition of 6 N HCl. The title compound was extracted three times with dichloromethane (3 mL × 30 mL). The combined organic layers were dried over magnesium sulfate, and the filtrate was concentrated under reduced pressure. The residue was crystallized in methanol−water (yield: 80−85%).

Effect on AMPA-Evoked Membrane Depolarization (*in Vitro* Fluorescence Assay). This assay was performed on rat primary brain cultures using fluorescent membrane potential dyes and an imaging-based plate reader (FDSS, Hamamatsu, JP) following our previously published procedure.[16,19]

Effect on AMPA-Mediated Release of Noradrenaline on Rat Hippocampal Slices. Potentiation of noradrenaline release on rat hippocampal slices was measured according to our previously reported procedure.[20,21]

Protein Expression and Purification. The dimeric GluA2-LBD double mutant L483Y−N754S was expressed and purified as previously described.[22] Briefly, *Escherichia coli* Origami B (DE3) cells were transformed with the GluA2−LBD−L483Y−N754S pET-22b(+) plasmid. Cells were grown in LB medium to an OD_{600} of 0.9 where the cells were subsequently cooled on ice to 20 °C. Protein expression was induced by addition of 0.5 mM isopropyl β-D-thiogalactopyranoside. Cells were harvested and lysed after 18 h, and the soluble protein was initially purified by Ni^{2+}-affinity chromatography. The *N*-terminal His-tag was cleaved by tryptic digest, and the cleaved protein was further purified by anion-exchange chromatography and size-exclusion chromatography.

Isothermal Titration Calorimetry. An ITC200 Micro-Calorimeter (GE Healthcare) with a cell volume of 200 μL was used for ITC at 25 °C. Titrations with **5b**, **5d**, and **6** were direct titrations, whereas the binding affinity of **5a** was determined in a displacement assay with **5c**. The protein solution consisted of GluA2−LBD−L483Y−N754S in 100 mM HEPES, 100 mM NaCl, 2 mM KCl, 5 mM L-glutamate, and pH 7.0. UV absorption was used to determine the protein concentration, which was 47 μM (**5b** titration), 31 μM (**6** titration), 29 μM (**5d** titration), and 20 μM (**5a** titration). The protein solution buffer was also used to dissolve the compounds to the following concentrations used for ITC: 695 μM **5b**, 490 μM **6**, and 543

dx.doi.org/10.1021/ci500559b | J. Chem. Inf. Model. 2014, 54, 3404−3416

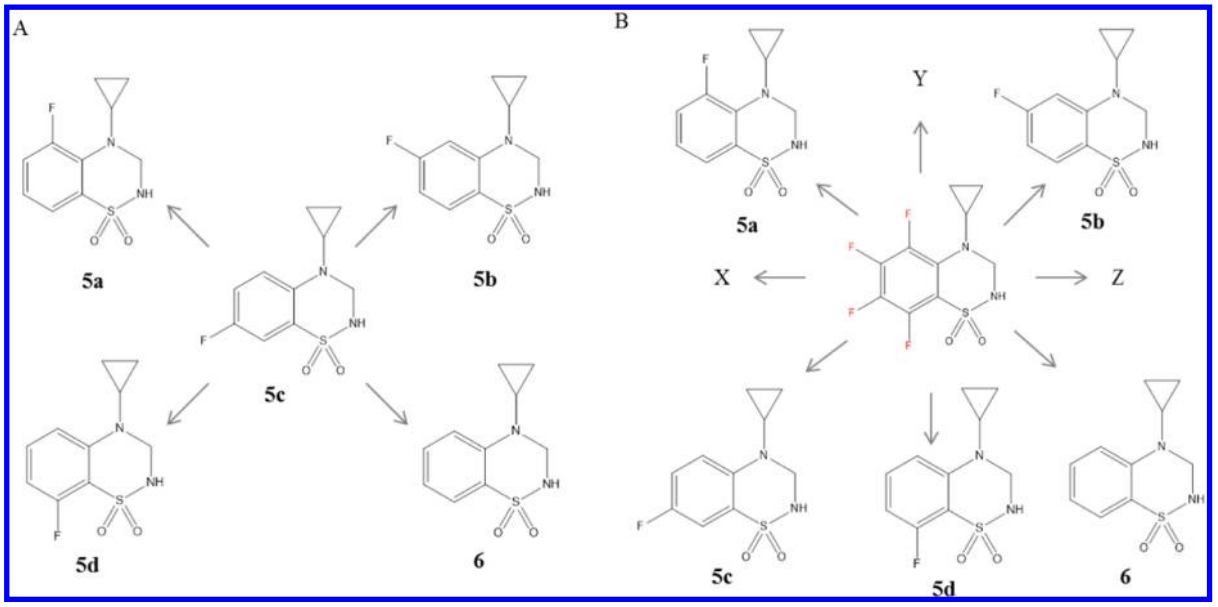

Figure 4. Schematic overview of the thermodynamic integration (TI) and one-step perturbation (OSP) simulations. (A) TI simulations. Each TI simulation starts with **5c** (λ = 0) and simulates the perturbation to **5a**, **5b**, **5d**, or **6** (λ = 1), respectively. (B) OSP simulation of a reference compound with four soft fluorine atoms (marked in red). From a single simulation of the reference compound, the difference in free energy relative to each of the real compounds (**5a**, **5b**, **5c**, **5d**, and **6**) can be calculated as well as predictions for other compounds represented by the references state, here marked by X, Y, and Z.

μM **5d**. For the displacement ITC assay of **5a** with **5c**, 285 μM **5c** was used to displace 100 μM **5a**. All experiments were set up with 20 injections with 3 min intervals; first injection was 0.4 μL, the remaining 2 μL. Data analysis was performed using the Origin 7.0 software (MicroCal) (single binding site model). For each binding curve, the first data point was discarded, and the heat of dilution of injecting ligand into the buffer was subtracted prior to fitting. All experiments were performed three times, and the reported K_d, ΔH, and $-T\Delta S$ are mean values of three independent titrations.

Simulation Setup. The GROMOS11 suite of simulation programs was used for all simulations.[23] The GROMOS++ suite of programs was used to set up and analyze the simulations.[24]

The coordinates for the protein were extracted from the crystal structure of GluA2−LBD−L483Y−N754S in complex with BPAM97 at 1.95 Å (PDB code 3TDJ; the X-ray structure of GluA2−LBD−L483Y−N754S in complex with BPAM344 was not available when the simulations were initiated).[22] The GROMOS 54a8 force field was applied for MD simulations.[25] The endogenous ligand *L*-glutamate was described according to the same force field in the zwitter-ionic form and bearing a net charge of −1 *e*. Building blocks for the allosteric modulators were derived from similar functional groups available in the force field. In particular, the sulfonamide group was previously described in simulations of sildenafil,[26] and the charge distributions for the fluorine substituents are taken from a model of trifluoroethanol.[27] The building blocks of all species are available in the Supporting Information. For the protein, all Glu, Asp, Lys, and Arg residues were described in their charged states, while the optimal protonation states of His (neutral) were chosen such that the potential number of hydrogen bonds is maximized.

The protein−ligand complex was placed in a rectangular box with a size of 7.8 nm × 8.7 nm × 9.9 nm with a minimum solute−solvent distance of 0.23 nm, with 13 Cl^- and 5 Na^+ ions added and containing approximately 19,000 simple point charge (SPC) water molecules. To obtain the free-energy differences of the free compounds in water, which are required to calculate the free energy of binding, all real compounds and the reference compound (see below) were also simulated free in solution. For this, a box with 727 SPC water molecules was used.

To relax unfavorable contacts between the protein−ligand complex and the solvent or ligand and solvent, all systems were energy minimized before simulations, using a steepest descent energy minimization with an energy threshold of 0.1 kJ mol^{-1}. Initial velocities were subsequently assigned randomly from a Maxwell−Boltzmann distribution corresponding to 60 K. In the thermalization and equilibration phase, the temperature was gradually increased from 60 to 300 K using the weak coupling scheme[28] over six discrete simulation steps, while decreasing the force constant of an initial positional restraint from 25000 kJ mol^{-1} nm^{-2} to zero. In the seventh step, the Nosé−Hoover chains algorithm[29] was used involving three chains and a reference temperature of 300 K.

Preliminary simulations showed rotations of the modulators up to ±90° relative to the crystal structure, and therefore, a distance restraint was applied between the center of geometry of C4, C6, and C10 of one modulator to the F2 on the other modulator with an optimal distance of 0.36 nm and a force constant of 4000 kJ mol^{-1} nm^{-2} (for atom numbering, see the molecular building blocks in the Supporting Information).

All production simulations were performed with a constant volume, constant temperature (300 K), and constant number of particles. Stability of the simulations was confirmed by calculating the atom-positional root-mean-square deviations with respect to the initial starting structure and by monitoring the occurrence of hydrogen bonds and secondary structure elements over the course of the simulations. The presence of hydrogen bonds was determined using a geometric criterion requiring a maximum hydrogen−acceptor distance of 0.25 nm

and a minimum donor−hydrogen−acceptor angle of 135°.[30] The occurrence of secondary structure elements was determined using the Kabsch−Sander rules,[31] as implemented in the GROMOS++ suite of analysis programs.

Free Energy Calculations. The relative free energy of binding between two compounds A and B can be calculated using a thermodynamic cycle,[32] from which the following equations can be derived

$$\Delta\Delta G_{\text{bind}} = \Delta G_{\text{bind}}(\text{B}) - \Delta G_{\text{bind}}(\text{A}) = \Delta G_{\text{AB}}(\text{prot}) - \Delta G_{\text{AB}}(\text{wat}) \quad (1)$$

where ΔG_{bind} (B) and ΔG_{bind} (A) represent the binding free energy of compound B and A, respectively, and ΔG_{AB} is the free energy of changing compound A into compound B as calculated in the protein (prot) or free in solution (wat).

Thermodynamic Integration. In thermodynamic integration (TI), ΔG_{AB} is calculated by gradually modifying compound A into compound B using a coupling parameter, λ, which connects the Hamiltonians describing the two compounds. The Hamiltonian, $H(\lambda)$, is parametrized such that at $\lambda = 0$ it represents compound A ($H(0) = H^{\text{A}}$), and at $\lambda = 1$ it represents compound B ($H(1) = H^{\text{B}}$). Here, the GROMOS parametrization of the Hamiltonian is used[33] with a softcore potential[34] with softness parameters $\alpha_{\text{LJ}} = 0.5$ and $\alpha_{\text{CRF}} = 0.5$ nm^2.

The derivative of the Hamiltonian with respect to λ is calculated at each λ point, and the ensemble average is numerically integrated providing the free energy difference between compounds A and B.[35] In the current work, performed at constant volume, we calculate the Helmholtz free energy difference, ΔA. For the small alchemical changes described here, the volume−pressure work will be negligible, and the Helmholtz and Gibbs free energies will be directly comparable.

$$\Delta G \approx \Delta A = \int_{\lambda=0}^{\lambda=1} \left\langle \frac{\partial H(\lambda)}{\partial \lambda} \right\rangle d\lambda \quad (2)$$

In practice, the ensemble average, $\langle \partial H(\lambda)/\partial\lambda \rangle$, is calculated from at least 11 independent simulations performed at 11 equidistant λ values. At every λ value, a short equilibration was performed for 100 ps, followed by production simulations of at least 1 ns. To obtain a smooth TI curve, up to three additional simulations were performed at intermediate λ values. The free energy differences between the allosteric modulators were calculated as outlined in Figure 4A for the compounds free in solution and while bound to the protein. In the protein simulations, both modulators were modified simultaneously, with a distance restraint between them. The ensemble averages were unbiased prior to the integration as in umbrella sampling[36,37] using

$$\left\langle \frac{\partial H}{\partial \lambda} \right\rangle_{\text{ub}} = \frac{\left\langle \frac{\partial H}{\partial \lambda} e^{U_{\text{bias}}/k_{\text{B}}T} \right\rangle_{\text{b}}}{\left\langle e^{U_{\text{bias}}/k_{\text{B}}T} \right\rangle_{\text{b}}} \quad (3)$$

where U_{bias} is the energy of the restraint, subscript "b" indicates the ensemble averages obtained in the presence of the bias, subscript "ub" indicates the ensemble average in the unbiased case, k_{B} is the Boltzmann constant, and T is the absolute temperature.

One-Step Perturbation. To estimate the free energy difference using OSP,[38] a reference molecule, which can sample the relevant phase space for all real compounds, was designed (Figure 4B). The challenge lies in designing the reference compound to have the best possible resemblance to all real compounds.[18] The reference compound contains four soft fluorine atoms for which the charge was set to 0, and the van der Waals interaction was softened[34] to remove the singularity at the origin with a softness parameter of $\alpha_{\text{LJ}} = 1.51$.[39]

To calculate the free energy difference between a real compound and the reference compound, the Zwanzig perturbation formula was applied to a single simulation of the reference state.[40] Thus, the free energy difference between a real compound, A, and the reference compound, R, is calculated via

$$\Delta A_{\text{RA}} = A_{\text{A}} - A_{\text{R}} = -k_{\text{B}}T \ln\langle e^{-(H^{\text{A}}-H^{\text{R}})/k_{\text{B}}T} \rangle_{\text{R}} \quad (4)$$

where angular brackets indicate the ensemble average obtained using molecular dynamics (MD) simulation of the reference compound, R. Again, in view of the small perturbations considered here, we use the approximation $\Delta G_{\text{RA}} \approx \Delta A_{\text{RA}}$. In this particular case H^{R} also contains the restraining energy between the two reference molecules, such that the free energy of releasing the restraint is included in ΔG_{RA}. The free energy difference between the real compounds is subsequently calculated according to $\Delta G_{\text{AB}} = \Delta G_{\text{RB}} - \Delta G_{\text{RA}}$. Production simulations of the reference state free in solution and when bound to the protein were performed for 10 ns, writing the coordinates every 0.5 ps for later analysis.

Enthalpy−entropy Compensation. Theoretically, the enthalpic and entropic contributions to the relative binding free energies are also accessible from the simulations. The enthalpy difference can be obtained from the difference in the average total energy for two compounds, incremented by the volume−pressure work

$$\Delta H^{\text{AB}} = \langle H^{\text{B}} \rangle_{\text{B}} - \langle H^{\text{A}} \rangle_{\text{A}} + V\Delta p \quad (5)$$

where $\langle H^{\text{A}} \rangle_{\text{A}}$ and $\langle H^{\text{B}} \rangle_{\text{B}}$ indicate the ensemble average of the Hamiltonian of compound A and B, respectively, as calculated over the ensemble for compounds A and B. The volume−pressure work as appropriate in simulations in the NVT ensemble and due to the alchemical modifications described in this work will be negligible. The entropy is subsequently calculated from the difference between the enthalpy and free energy.[41]

However, eq 5 is known to converge poorly, as it is based on the total energy of the entire system. Still, for a pairwise additive force field, the total enthalpic change can be divided into the contributions due to the ligand and its surroundings as well as the contributions due to the interactions within the surroundings (protein and solvent).

$$\Delta H_{\text{ls}}^{\text{AB}} = \langle H_{\text{ls}}^{\text{B}} \rangle_{\text{B}} - \langle H_{\text{ls}}^{\text{A}} \rangle_{\text{A}} \quad (6)$$

with H_{ls} describing the ligand-surrounding energy terms of the Hamiltonian. It can be proven that the surrounding−surrounding enthalpies are explicitly included in the corresponding entropy change, largely explaining the often-observed enthalpy−entropy compensation.[15] The reduced term ΔH_{ls} does not correspond to an experimental observable but can be considered as the direct enthalpic driving force. Moreover, it can be readily computed from molecular simulations and may help to dissect the origins of the experimentally determined thermodynamic quantities. Equation 6 was applied directly to the end-state simulations of the TI calculations.

dx.doi.org/10.1021/ci500559b | J. Chem. Inf. Model. 2014, 54, 3404−3416

Table 1. Effects of Monofluoro-Substituted 4-Cyclopropyl-3,4-dihydro-2*H*-1,2,4-benzothiadiazine 1,1-Dioxides on Depolarization Induced by 300 μM AMPA in Primary Neuronal Cultures from Rat Embryonic Cortex and on AMPA-Mediated Presynaptic Noradrenaline (NA) Release on Rat Hippocampal Slices

	AMPA-mediated depolarization			
compound	EC_{2x}[a] (μM)	E_{max}[b]	EC_{50}[c] (μM)	AMPA-mediated NA rel.[d] (%)
5a	2.14 [1.55; 2.96] (5)	>x7.20 ± 1.02 (5)	ND	320.63 ± 24.51 (4)
5b	2.11 [1.01; 4.39] (3)	x5.67 ± 0.33 (3)	6.69 [2.74; 16.34] (3)	363.44 ± 12.02 (2)
5c[e]	0.26 [0.15; 0.47] (3)[e]	x15.00 ± 2.65 (3)[e]	0.89 [0.53; 1.48] (3)[e]	330.33 (1)
5d	0.33 [0.22; 0.50] (3)	x11.67 ± 1.76 (3)	1.44 [0.61; 3.43] (3)	373.46 ± 21.97 (2)
6[e]	0.70 [0.30; 1.67] (3)[e]	x8.50 ± 0.76 (3)[e]	4.07 [2.08; 7.96] (3)[e]	394.37 (1)

[a]EC_{2x}: concentration of modulator giving a 2-fold increase of the depolarization induced by 300 μM AMPA. [b]E_{max}: maximal effect obtained by compounds in the presence of 300 μM AMPA, normalized to unity for response evoked in the presence of AMPA alone taken as x1. [c]EC_{50}: concentration of modulator responsible for 50% of the maximal effect. [d]NA rel.: effect of compounds on AMPA-mediated noradrenaline release at 300 μM, normalized to the effect obtained in the presence of AMPA alone, taken as 100%. For EC_{2x} and EC_{50} results are expressed as geometric mean and upper and lower confidence intervals. For E_{max} and NA release, results are expressed as mean and standard error to the mean. Numbers in brackets indicate the number of independent experiments. ND: not determined. [e]Published compounds and results (see ref 16; in this previous publication, all results were expressed as the arithmetic mean, showing very small differences from the geometric means reported here).

RESULTS AND DISCUSSION

Chemistry. The synthesis of monofluoro-substituted 4-cyclopropyl-3,4-dihydro-2*H*-1,2,4-benzothiadiazine 1,1-dioxides **5** is described in Figure 3. The appropriate *o*-fluoroaniline **1** bearing a second fluorine atom in another position of the benzene nucleus was converted into the corresponding *o*-fluorobenzenesulfonamide **2** by means of the Meerwein variation of the Sandmeyer diazotization reaction.[42] Nucleophilic substitution of the fluorine atom of intermediates **2** by cyclopropylamine, providing the corresponding 2-cyclopropylaminobenzenesulfonamides **3**, was performed in a closed vessel by heating the mixture at 130−150 °C for 24−48 h. The use of *o*-fluorobenzenesulfonamides instead of the corresponding *o*-chlorobenzenesulfonamides was preferred because of the greater reactivity of fluoro-substituted aromatic compounds to nucleophilic substitution. Moreover, this reaction was greatly facilitated by the fact that the fluorine atom was located at the *ortho* position of the electron-withdrawing sulfonamide group. In the case of intermediate **2b**, which bears a fluorine atom in the *para* position of the sulfonamide group and is thus in competition with the *ortho* position for the reaction with the amine, the nucleophilic substitution was mainly observed in the *ortho* position. Ring closure of intermediates **3** by heating them in triethyl orthoformate provided fluoro-substituted 4-cyclopropyl-4*H*-1,2,4-benzothiadiazine 1,1-dioxides **4**, which were converted with sodium borohydride into the corresponding "saturated" final compounds **5**. The characterization of all compounds is given in the Supporting Information.

Biological Evaluation. The new fluoro-substituted BTD compounds **5a** (5-F), **5b** (6-F), and **5d** (8-F) were evaluated as AMPA receptor potentiators in an *in vitro* fluorescence assay, and their activity was compared to that of the previously reported BTD compound **5c** (7-F) as well as the unsubstituted analogue **6**.[16] The experiments were performed on primary cultures of neurons from rat embryonic cortex, measuring the effect of the modulators on AMPA-evoked membrane depolarization, as previously described.[16,19] For each compound, the EC_{2x} value was determined (concentration of modulator giving a 2-fold increase of the fluorescence induced by 300 μM AMPA), as well as their maximum effect (E_{max} value normalized to unity for AMPA-evoked response taken as x1) (Table 1). It was observed that the 8-fluoro-substituted compound **5d**, with an EC_{2x} value of 0.33 μM and a high value of maximal potentiation of x15, exhibited a potentiator effect on AMPA receptors comparable to that of the 7-fluoro-substituted reference compound **5c**,[16] while their 5- and 6-fluoro-substituted analogues, although very active (EC_{2x} ∼ 2 μM), were clearly less efficient. This result indicated that the best positions for a fluorine atom on the BTD ring system are the 7- and 8-positions. Such an observation was already made with their corresponding monochloro-substituted BTDs. However, the fluoro-substituted analogues were systematically found to be more active on AMPA receptors than the corresponding chloro-substituted compounds.[43]

It is known that positive allosteric modulators of the AMPA receptor are able to potentiate noradrenaline (NA) release in rat hippocampal slices, an effect linked to their interaction with presynaptic AMPA receptors.[21,44] At 300 μM, most of the compounds induced a strong enhancement of the (*S*)-AMPA (10 μM) evoked [^{3}H]-NA release (100% representing the effects shown by (*S*)-AMPA alone). This result indicated that the new monofluoro-substituted compounds **5a**, **5b**, and **5d**, as previously observed with compounds **5c** and **6**,[16] were able to act on presynaptic AMPA receptors, almost with the same efficacy.

Thermodynamic Details of Modulator Binding. To measure modulator binding independently of dimer formation, we used a double mutant of the GluA2 LBD, GluA2-LBD−L483Y−N754S. This mutant is a preformed dimer in solution, which mimics the endogenous binding environment found in the dimer of dimers structure of the full-length GluA2 receptor. We have previously used this mutant for ITC measurements, and the mutations do not interfere with modulator binding.[16,22]

For compounds **5b**, **5d**, and **6** the thermodynamic details of binding were determined in a direct titration with GluA2. For **5a**, we were not able to measure a saturation curve in a direct titration, and therefore, the thermodynamic properties were determined in an ITC displacement assay with the previously reported **5c**.[16] The ITC experiments showed that for all four compounds, binding is an exothermic process (Figure 5). The binding affinities (K_d) and thermodynamic quantities are given in Table 2. The following rank order in binding affinity (K_d) was observed, with the most potent compound listed first: **5c** (7-F) > **5d** (8-F) > **6** (no-F) > **5b** (6-F) > **5a** (5-F). For compound **6**, the complex formation is primarily enthalpy driven as also previously seen for **5c**. On the contrary, the complex formation for **5a** and **5b** is primarily entropy driven,

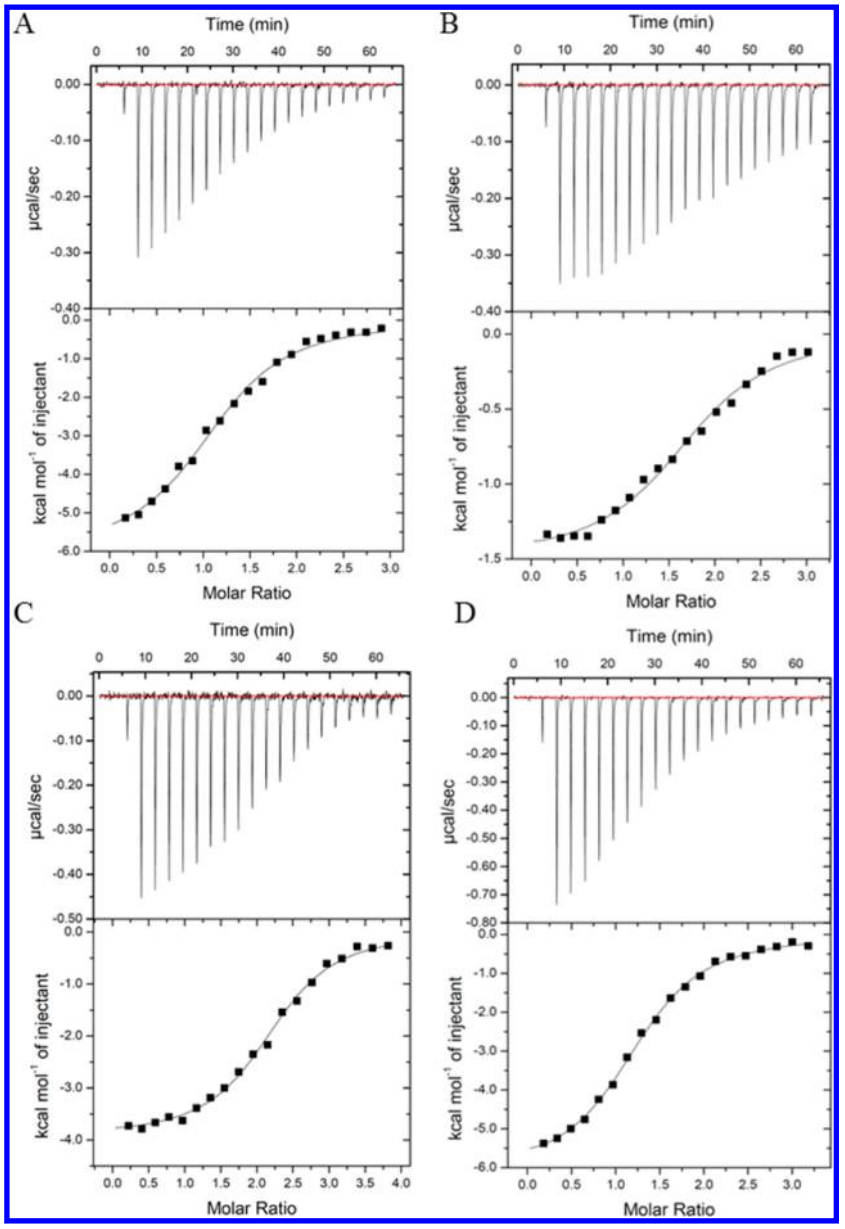

Figure 5. Isothermal titration calorimetry study of binding of **5a** (A), **5b** (B), **5d** (C), and **6** (D) to GluA2−LBD−L483Y−N754S. Top panel shows raw data, and the bottom panel shows the derived isotherm. Heat is developed after each injection (exothermic reaction), and the signal is reduced during saturation of the protein with (A) **5c** (for displacement of **5a**), (B) **5b**, (C) **5d**, and (D) **6**. The shown experiments are a representative of three independent experiments.

Table 2. Isothermal Titration Calorimetry on Modulator Binding to GluA2−LBD−L483Y−N754S

	5a[b]	**5b**	**5c**[a]	**5d**	**6**
K_d (μM)	12.3 ± 1.9[c]	7.0 ± 0.6	0.35 ± 0.02	2.8 ± 0.6	3.9 ± 0.4
ΔG_{bind} (kJ/mol)[d]	−28.0 ± 0.4	−29.4 ± 0.2	−36.8 ± 0.1	−31.7 ± 0.5	−30.8 ± 0.3
ΔH (kJ/mol)	−10.0 ± 2.1	−7.9 ± 1.3	−31.4 ± 0.8	−17.9 ± 0.4	−25.1 ± 1.3
$-T\Delta S$ (kJ/mol)	−18.0 ± 2.1	−21.8 ± 1.7	−5.4 ± 0.8	−15.1 ± 0.8	−5.9 ± 1.3
n_H[e]	nd[f]	1.7 ± 0.1	2.7 ± 0.1	2.2 ± 0.2	1.4 ± 0.1

[a]Values from ref 16. [b]Thermodynamic properties of **5a** were determined in an ITC displacement assay with **5c**. [c]Standard deviation over three independent experiments. [d]Calculated from $\Delta G = RT \ln(K_d)$, [e]Stoichiometry, [f]Not determined.

whereas the **5d** complex formation is equally enthalpy and entropy driven (Table 2).

To decipher the mode of action of the modulators, we compared the relative difference in EC_{2x} for a compound **x** (EC_{2x}(**x**)/EC_{2x}(**5c**)) with the relative difference in K_d: (K_d(**x**)/K_d(**5c**)). A direct comparison between EC_{2x} and K_d is not possible because EC_{2x} is the concentration of modulator that leads to 2-fold increase in receptor response to a given agonist compared to the agonist alone and only indirectly contains information on binding affinity. The comparison of the relative

dx.doi.org/10.1021/ci500559b | J. Chem. Inf. Model. 2014, 54, 3404−3416

differences in EC_{2x} to the ITC data enables a decomposition of the EC_{2x} values into the binding effect and modulatory strength. Thus, it suggests if the relative difference between the effects of two compounds is purely due to binding affinity or if it is due to a more efficient modulation. If $EC_{2x}(\mathbf{x})/EC_{2x}(\mathbf{5c})$ equals $K_d(\mathbf{x})/K_d(\mathbf{5c})$, it suggests that these compounds are different in their binding affinity only, and hence, the two compounds should have similar modulatory effects. If $EC_{2x}(\mathbf{x})/EC_{2x}(\mathbf{5c})$ does not equal $K_d(\mathbf{x})/K_d(\mathbf{5c})$, then binding affinity alone does not explain the differences, and therefore, the two compounds likely have different modulatory strengths. From data in Tables 1 and 2, it is seen that for all compounds the $EC_{2x}(\mathbf{x})/EC_{2x}(\mathbf{5c})$ is lower than $K_d(\mathbf{x})/K_d(\mathbf{5c})$. Thus, differences in the binding affinity between the modulators are most likely not the sole cause of the difference between these compounds. The largest difference is seen for **5a** relative to **5c**, where $K_d(\mathbf{5a})/K_d(\mathbf{5c})$ amounts to 35, while $EC_{2x}(\mathbf{5a})/EC_{2x}(\mathbf{5c})$ is only 8. The other three compounds show smaller differences between the fractions. This suggests that **5a** may have a stronger modulatory effect than **5c**, which is partially compensated by a weaker binding of **5a** relative to **5c**. Therefore, it may be of interest to improve the binding affinity by introducing modifications elsewhere in **5a**.

Stability of Simulations. To set up a system for calculation of binding affinities, we used the GluA2−LBD−L483Y−N754S protein in complex with either two copies of **5c** for TI (Figure 4A) or two copies of the reference molecule for OSP (Figure 4B).

To ensure that the MD simulations represent stable protein structures, we evaluated the root-mean-square (RMS) deviation of the protein backbone from the initial starting structure. The RMS deviation remained below 0.25 nm, which indicates stability of the protein. Furthermore, the average occurrence of hydrogen bonds as well as the occurrence of secondary structural elements remained stable throughout the simulations (data not shown). However, a closer inspection of modulator binding in the protein showed that the modulators were turning ±90° relative to the crystal structure of GluA2−LBD−L483Y−N754S with **5c** (PDB code 4N07) in all MD simulations. Therefore, we used two distance restraints between the two modulator molecules located at the binding site from the fluorine atom of one modulator to the center of geometry on the benzene ring of the other modulator and *vice versa* (see Materials and Methods).

Free Energy Calculations. The results of the free energy calculations using both TI and OSP are shown in Table 3 along with the relative free energy differences calculated from ITC. As a consistency check, the free energy differences from **5d** to **5a**, from **5a** to **6**, from **6** to **5b**, and from **5b** to **5d** were calculated in water as well, and the maximum free energy difference along the closed cycles was −0.19 kJ/mol. Comparing the relative free energy calculated by TI with the free energy determined by ITC, we get a RMS error of 5.1 kJ/mol, which is slightly higher than what is typically considered "chemical accuracy" (∼4 kJ/mol)[45] but just below 5.6 kJ/mol corresponding to a factor 10 in K_d at room temperature. This high RMS error of the TI calculations is primarily due to the poor prediction of **5a** relative to **5c** (−0.4 kJ/mol vs 8.8 kJ/mol determined by ITC), but also the prediction for **6** is relatively poor (2.5 kJ/mol vs 6.0 kJ/mol), although still within chemical accuracy.

Next, we calculated the free energy of binding using the OSP method, which is a computationally more efficient method than TI. When we compare the OSP free energy calculations with the relative free energy differences from ITC, we obtain a RMS error of 2.1 kJ/mol, which is even below thermal fluctuations (k_BT = 2.5 kJ/mol). Thus, for this series of compounds, we find that the OSP setup gives better predictions. Similar to the TI calculations, the relative free energy of binding of **5a** was the most difficult to calculate (11.9 kJ/mol vs 8.8 kJ/mol). However, the OSP method performs slightly better than the TI method for the difference between **5c** and **6** and conversely slightly worse for **5b**.

Thus, the calculations of the relative binding free energy of **5a** showed the poorest correlation for both TI and OSP in comparison to the experimentally determined relative free energies from ITC. For this setup, we found the OSP method to have a somewhat higher predictive power compared to the TI method. This is promising because for the four TI calculations in Figure 4A, we have performed at least 4 ns × 11 ns × 1 ns = 44 ns of simulation, while the OSP calculations are based on a single simulation of 10 ns of the reference state.

Ligand Orientations, Conformations, and Interactions. The modulators bind in the dimeric interface of the GluA2 ligand binding domain. The only direct hydrogen bond observed is between the N2 hydrogen and the carbonyl oxygen of Pro494 (Figures 1B and C).[16,22] For **5c** and its analogue BPAM97, a weak hydrogen−fluorine bond has been observed to Ser497, otherwise the binding of the modulators is stabilized primarily through nonbonded interactions and shape complementarities. To check that the experimentally observed binding pose was also seen in the simulations, we examined the final structures from the end-state simulations of the TI and compared them to the experimentally observed structure of **5c** (Figure 6). The structures of **5b** and **6** match best with the experimental structures for both copies of the modulators (Figure 6A and C). An alternative puckering of the ring system relative to the experimental structure was observed for **5d** in one of the modulators (Figure 6B). The puckering seen in the crystal structure enables the only hydrogen bond from the N2 hydrogen of the modulator to the carbonyl oxygen of Pro494.

The advantage of the OSP method lies in the usage of a reference structure, which may sample all relevant conformations of multiple molecules of interest. For the OSP calculations, the number of structures in the trajectories that contribute significantly to the free energy calculation was determined for each real compound by counting the number of structures for which the energy difference $H^A - H^R$ in eq 4 was less than the final free energy difference increased by k_BT ($H^A - H^R < \Delta G_{AR} + k_BT$). The number of contributing structures was found to be in the range of 0.3−12% of the entire set of

Table 3. Relative Free Energies of Modulator Binding to GluA2−LBD−L483Y−N754S[a]

Compound	$\Delta\Delta G_{bind}$ (ITC)	$\Delta\Delta G_{bind}$ (TI)	$\Delta\Delta G_{bind}$ (OSP)
5a	8.8	−0.4	11.9
5b	7.4	5.9	5.0
5c	0.0	0.0	0.0
5d	5.1	7.2	6.3
6	6.0	2.5	4.9
RMS error	−	5.1	2.1

[a]All values (in kJ/mol) are denoted as the free energy relative to **5c** as this was the compound for which the X-ray structure was solved and that is central in the TI calculations (Figure 4A).

dx.doi.org/10.1021/ci500559b | J. Chem. Inf. Model. 2014, 54, 3404−3416

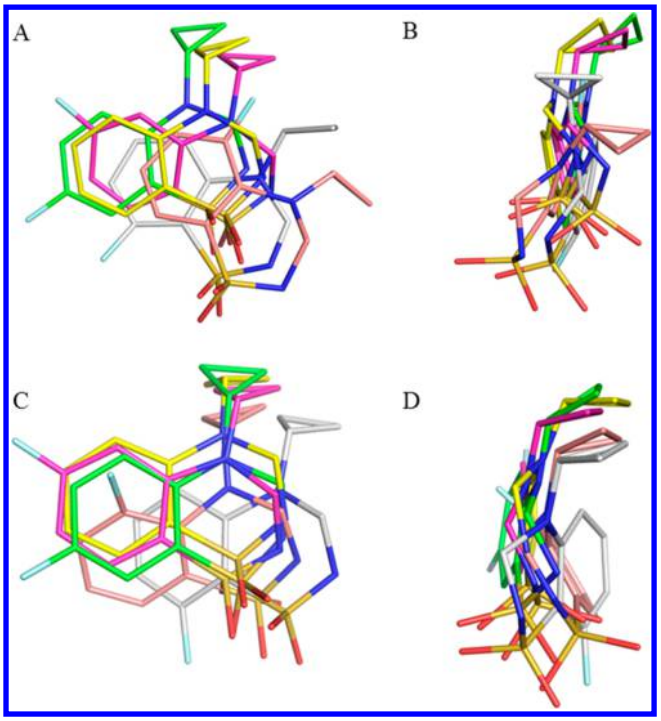

Figure 6. Binding mode of modulators in TI end-state simulations. Structures of **5a**, **5b**, **5d**, and **6** from TI end-state simulations are shown in line representation with the X-ray crystal structure of **5c** in complex with GluA2−LBD−L483Y−N754S (PDB code 4N07, green lines). Color code: **5a**, salmon; **5b**, magenta; **5d**, gray; and **6**, yellow. (A) Front view of BTD molecule 1. (B) Side view of BTD molecule 1. (C) Front view of BTD molecule 2. (D) Side view of BTD molecule 2.

20,000 structures, with the lowest amount of structures contributing to the free energy estimates of compound **5a**.

We extracted the single structure, which contributed the most to the free energy calculation for each of the real compounds from the OSP simulation. Figures 7A and C show the front view of the single structures with the highest probability for each of the compounds in line representation together with the X-ray crystal structure of **5c** in complex with GluA2−LBD−L483Y−N754S. The RMS deviations of the most contributing ligand structures were found to be 2.4 Å (**5a**), 1.3 Å (**5b**), 0.95 Å (**5c**), 2.6 Å (**5d**), and 1.1 Å (**6**), with respect to the X-ray structure of **5c**. For both copies of the compounds, some translation of the simulated structures relative to the crystal structure (in green) is seen; the best overlap with the X-ray structure is seen for **5c** and **6** (Figures 7A and C).

The side view of the same structures reveals a different puckering of the ring system for **5a** and **5d** in both copies of the modulator (Figures 7B and D) relative to the puckering observed in the X-ray structure of **5c**. The observation of both conformations indicates that the reference structure simulates a broad ensemble of conformations, and the relevant structures for the individual compounds may be selected. Furthermore, the cyclopropyl group is rotated 180° for **5a** and **5d** (Figures 7B and D) and 90° for **5b** (Figure 7B) relative to the conformation seen in the X-ray crystal structure of **5c** in GluA2−LBD−L483Y−N754S.

We also calculated the average puckering for the real compounds by reweighting the reference state simulation (data not shown) and confirmed our observations of the single highest contributing structures. Comparing the results from the

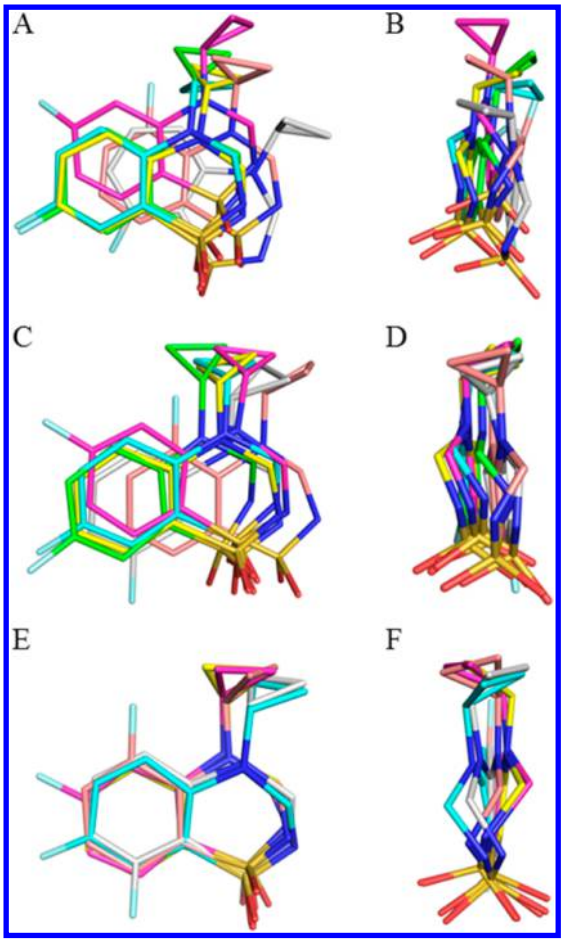

Figure 7. Overlay of the most contributing structures of the real compounds from the OSP simulation. Most contributing structure of each real compound is shown in line representation along with the X-ray crystal structure of **5c** in complex with GluA2−LBD-L483Y−N754S (PDB code 4N07, green lines). Color code: **5a**, salmon; **5b**, magenta; **5c**, cyan; **5d**, gray; and **6**, yellow. (A) Front view of BTD molecule 1. (B) Side view of BTD molecule 1, (C) Front view of BTD molecule 2. (D) Side view of BTD molecule 2. (E) Front view of BTD compounds from OSP simulation in water. (F) Side view of BTD compounds from OSP simulation in water. The figure was prepared using PyMOL (PyMOL Molecular Graphics System, version 1.5.0.5, Schrödinger, LLC).

TI and OSP, it is seen that **5a** consistently goes to the alternative puckering in the OSP, while it remains in the experimentally observed puckering in the TI calculations. This may explain the differences observed between the free energy values using TI and OSP (Table 3).

To see if the two different ring conformations represent an intrinsic effect of the compounds or if they are induced by the protein, we also extracted the highest contributing structure for each of the real compounds from the simulation in water (Figures 7E and F). Here, the two different ring conformations were also observed, where **5c** and **5d** showed preference for the conformation seen in the crystal structure, and **5a**, **5b**, and **6** were found with the other ring conformation. The observation of both conformations in the water simulation suggests that there is not a large energy difference associated with the transition in water, and thus, the protein may easily influence the preference for either of the conformations. **5c** and **5a** are the only compounds that preserve the intrinsic conformation seen in the water simulation when bound to the protein. For

dx.doi.org/10.1021/ci500559b | J. Chem. Inf. Model. 2014, 54, 3404−3416

5b, **5d**, and **6**, the binding to the protein may result in a slightly shifted orientation, which induces another puckering than seen in the water simulation (considering only the single most contributing structure). For **5a**, the fluorine substituent may influence the puckering by some steric hindrance caused by the cyclopropyl group, thus favoring the alternative conformation to the X-ray structure both intrinsically and in the protein, severely hampering the formation of the N2 hydrogen bond to the carbonyl oxygen of Pro494 and possibly explaining the low number of contributing structures to its free energy estimate.

These observations suggest that **5c** shows the overall combined best modulatory effect and binding affinity because it is the only compound with preserved intrinsically favored conformation, which is also the optimal conformation for hydrogen bonding when bound to the protein. Furthermore, **5d** also shows the alternative puckering of the ring in the protein, and this ligand is shifted most to the right from the X-ray structure. This observation may give a molecular explanation for the previously suggested difference in modulation effects as compared to compounds **5a**, **5b**, and **5c**.

Enthalpy−entropy Compensation. To investigate the thermodynamic details of ligand binding to the protein, we extracted the ligand-surrounding enthalpies, ΔH_{ls}, from the end-states of the TI simulations according to eq 6 (Table 4). TI simulations were preferred over OSP simulation data because the endstate TI are simulations of the real molecules. By comparing the computed ligand-surrounding enthalpy to the values that were obtained experimentally, we computed the changes in enthalpy due to the reorganization in the surroundings (protein and solvent; ΔH_{ss}). For ease of comparison, we have also explicitly calculated the thermodynamic quantities relative to **5c** ($\Delta\Delta H$, $\Delta\Delta H_{ls}$, and $\Delta\Delta H_{ss}$).

Table 4. Reduced Enthalpy and Entropy Terms from TI Simulation in kJ/mol

	ΔH(ITC)	ΔH_{ls}(TI)[a]	ΔHss[b]	$-T\Delta S$(ITC)
5a	−10.0	−41.7	31.7	−18.0
5b	−7.9	−39.7	31.8	−21.5
5c	−31.4	−44.6	13.2	−5.4
5d	−17.9	−39.6	21.7	−13.8
6	−25.1	−37.9	12.8	−5.7
	$\Delta\Delta H$(ITC)[c]	$\Delta\Delta H_{ls}$(TI)[c]	$\Delta\Delta H_{ss}$[c]	$-T\Delta\Delta S$(ITC)[c]
5a	21.4	3.0	18.4	−12.6
5b	23.5	5.0	18.5	−16.1
5c	0.0	0.0	0.0	0.0
5d	13.5	5.0	8.5	−8.4
6	6.3	6.7	−0.4	−0.3

[a]Calculated from eq 6. [b]Calculated as $\Delta H_{ss} = \Delta H(\text{ITC}) - \Delta H_{ls}(\text{TI})$. [c]Relative to **5c**.

Comparing **6** with **5c**, we see that the $\Delta\Delta G$(ITC) of 6.0 kJ/mol is almost entirely explained by the ligand-surrounding enthalpy change ($\Delta\Delta H_{ls}$(TI) = 6.7 kJ/mol). Because also $-T\Delta\Delta S$(ITC) is almost zero, the surrounding-surrounding enthalpy is close to zero as well. Hence, for this compound, there is no significant reorganization of the surroundings, and the difference in affinity is explained from the direct interaction energy between the modulator and the protein. This is in line with the very similar position of **6** at the binding site compared to **5c** (Figure 7).

For **5d**, the $\Delta\Delta G$(ITC) is also very similar to the value of $\Delta\Delta H_{ls}$(TI) in Table 4 (5.1 vs 5.0 kJ/mol). However, here the experiment indicates that the difference in binding of **5d** relative to **5c** is the result of an unfavorable enthalpy ($\Delta\Delta H$(ITC) = 13.5 kJ/mol) and favorable entropy ($-T\Delta\Delta S$(ITC) = −8.4 kJ/mol). This effect entirely compensates the enthalpy change due to reorganization of the surroundings ($\Delta\Delta H_{ss}$ = 8.5 kJ/mol). So even if the experiment suggests entropic differences between the compounds, a closer analysis reveals that the enthalpic differences in the direct interaction ($\Delta\Delta H_{ls}$(TI)) may explain the differences in affinity.

Finally, for **5a** and **5b**, the entropically driven binding is compensated by an even larger value of $\Delta\Delta H_{ss}$. Also, for these compounds, the largest portion of $\Delta\Delta G$ may be explained from $\Delta\Delta H_{ls}$(TI), and the favorable entropic contributions are entirely compensated by enthalpically unfavorable reorganization of the surroundings. Thus, the combination of experimental data with the calculated ligand-surrounding enthalpies allows us to dissect the origin of the measured enthalpies and entropies and could give a better insight into the design of new compounds. It is arguably easier to design compounds that have more favorable ΔH_{ls} than to design compounds to have an effect on the reorganization of the surroundings or on a largely compensated entropy.

Thus, our calculations of the energetic contributions to ligand binding indicate that enthalpic and entropic differences for this modulator series have large (compensating) contributions from either solvent reorganization or interactions between the protein and the solvent. This also shows that the differences in the binding affinities are mostly explained from direct interactions between the ligands and their surroundings.

Prediction of Binding Affinities. The strength of the OSP method lies in the need for only a single simulation of the reference compound to cover multiple compounds of interest (Figure 4B). Therefore, to characterize the modulator binding pocket with respect to the 4-cyclopropyl-3,4-dihydro-2*H*-1,2,4-benzothiadiazine 1,1-dioxide modulator scaffold, we designed a series of additional fluorine derivatives and calculated the free energy of these compounds relative to compound **6** for ease of comparison (Table 5).

Apart from **5c**, the 6,7-di-F compound was predicted to have the most favorable free energy ($\Delta\Delta G_{bind}$ = −2.2 kJ/mol), and the fluorine substituted compound that was predicted to have the least favorable energy was the 5,6,7,8-tetra-F compound with $\Delta\Delta G_{bind}$ = 24.6 kJ/mol. Comparing the predicted relative free energy for all the compounds with a fluorine at the 5-position, the $\Delta\Delta G$ is 9−24 kJ/mol, whereas for the four remaining fluorine-substituted compounds, the $\Delta\Delta G$ is (−2)−3 kJ/mol (i.e., without fluorine in the 5-position). Thus, an electronegative substituent or hydrogen-bonding acceptor in the 5-position decreases the predicted binding affinity regardless of the number and position of other electronegative substituents, in line with the unfavorable binding of **5a** (calculated and experimental).

Table 5, combined with the OSP data described in Table 3, allows us to investigate if the contributions of the F substitutions are additive or not. The free energy of some compounds may be approximated, for example, for the 5,8-di-F compound (9.4 kJ/mol relative to **6**), which is very close to the sum of the relative free energies for **5a** (7.0 kJ/mol) and **5d** (1.4 kJ/mol). Further examples of compounds for which additivity holds reasonably well are the 6,8-di-F and the 6,7-di-F compounds, while additivity does not hold for the 5,7-di-F, 5,7,8-tri-F, 5,6,7-tri-F, or 5,6,7,8-tetra-F compounds. This

dx.doi.org/10.1021/ci500559b | J. Chem. Inf. Model. 2014, 54, 3404−3416

Table 5. Prediction of Relative Binding Free Energies Using OSP Relative to Compound 6

substitution pattern[a]				
R_5	R_6	R_7	R_8	$\Delta\Delta G_{bind}$ (kJ/mol)
H	H	H	H	0.0
F	H	H	H	7.0
H	F	H	H	0.1
H	H	F	H	−4.9
H	H	H	F	1.4
F	F	H	H	12.8
F	H	F	H	9.6
F	H	H	F	9.4
H	F	F	H	−2.2
H	F	H	F	2.8
H	H	F	F	0.3
F	F	F	H	18.1
F	F	H	F	13.2
F	H	F	F	10.7
H	F	F	F	2.5
F	F	F	F	24.6
CH_3	H	H	H	63.3
H	CH_3	H	H	1.8
H	H	CH_3	H	7.1
H	H	H	CH_3	16.0

[a]MD simulation of the reference compound for the OSP calculations was used to predict the free energy of binding relative to **6** for selected compounds with different substitution patterns (Figure 2).

indicates that the predictions generated from the OSP simulation are more thorough than a simple QSAR model, which can be derived from looking at only the monosubstituted compounds, and take into account the mutual influences of the substitutions.

To investigate the impact of a small nonpolar substituent on the binding affinity, we calculated the binding free energies relative to **6** for a series of monosubstituted methyl compounds (Table 5). From these four derivatives, it is seen that the 5-substituted compound binds with the least favorable energy ($\Delta\Delta G_{bind}$ = 63.3 kJ/mol). The predicted methyl derivative with the most favorable energy is the 6-methyl compound with $\Delta\Delta G_{bind}$ = 1.8 kJ/mol. Thus, for both monomethyl and monofluorine compounds, the 5-substituted position is predicted to result in the weakest binding compounds; however, the predictions indicate that it is more favorable to have an electronegative atom compared to a bulkier methyl substituent in this position. Also, for **5a** (the 5-F-compound), the lowest number of structures contributing to the OSP calculations was observed, and this molecule favors an alternative puckering. Therefore, an explanation may also be found in a steric clash of any type of substituent in this position, which may favor an alternative puckering of the ring system, which in turn prevents the hydrogen bond between the modulator and the protein.

Comparing **5b** (6-F, $\Delta\Delta G$ = 0.1 kJ/mol) with the compound with a methyl in the 6-position ($\Delta\Delta G$ = 1.8 kJ/mol) shows that the two compounds with a substituent in the 6-position bind with similar relative free energies; thus, at this position, there is no apparent preference for either a hydrophobic or electronegative substituent. For both the 7- and 8-positions it is more favorable to have an electronegative substituent than a hydrophobic substituent, and it may also be concluded that it is more favorable for a substituent to be located in the 7-position rather than the 8-position.

In summary, for the 5-, 7-, and 8-positions, it is less favorable to fill up space with a hydrophobic substituent than to introduce an electronegative substituent, with the largest effect seen for the 5-position. For the 5-position, this may be due to interactions with the cyclopropyl group, leading to an alternative puckering. For the 7- and 8-positions, steric clashes with the protein environment cause unfavorable interactions. In contrast, for the 6-position, the difference between a methyl and an electronegative substituent is small. The 6-position is the position where a substituent would be the closest to its similar substituent on the other modulator molecule when bound to the protein, and thus, a substituent in this position might strengthen interactions between the modulators.

CONCLUSION

This work is the first example of combining experimental and calculated free energies of positive allosteric modulator binding to the GluA2 LBD, and furthermore, it gives a detailed decomposition of the thermodynamic driving forces of modulator binding.

The experimentally measured thermodynamic details of binding of this fluorine-substituted series of GluA2 positive allosteric modulators showed that despite similarities in the binding affinities complex formation was primarily enthalpy driven for **6** as also previously seen for **5c**. The **5a** and **5b** complex formation was primarily entropy driven, and **5d** complex formation was equally enthalpy and entropy driven. Dissection of the thermodynamic contributions, however, indicated that the main driving forces of the binding stem from the ligand-surrounding enthalpies for all compounds and that the experimentally determined enthalpic and entropic differences are largely explained by reorganizations in the protein and the solvent. Our comparison of the ITC, pharmacological, and simulation data suggested that because **5c** is the only compound, which preserves the intrinsically favored and optimal conformation for hydrogen bonding when bound to the protein, it shows the overall best combined modulatory effect and binding affinity. Our predictions generated using the OSP simulation provided an indication of favorable substitution positions in this modulator scaffold. While a larger substituent in the 5-, 7-, or 8-positions would be sterically unfavorable, a larger substituent in the 6-position might strengthen interactions between the modulators.

ASSOCIATED CONTENT

Supporting Information

Experimental characterization of intermediates and synthesis products, free energy profiles for TI, and molecular building blocks for all simulated compounds. This material is available free of charge via the Internet at http://pubs.acs.org.

AUTHOR INFORMATION

Corresponding Author

*E-mail: chris.oostenbrink@boku.ac.at.

Notes

The authors declare no competing financial interest.

ACKNOWLEDGMENTS

The Danish Council for Independent Research (Mobility Ph.D. grant) and GluTarget (A.B.N., L.O., J.S.K.), Vienna Science and

Technology Fund (WWTF, Grant LS08-QM03, C.O.), and European Research Council (ERC Grant 260408, C.O.) are acknowledged for financial support.

■ ABBREVIATIONS

ADHD, attention deficit hyperactivity disorder; AMPA, α-amino-3-hydroxy-5-methylisoxazole-4-propionic acid; BTD, 3,4-dihydro-2*H*-1,2,4-benzothiadiazine 1,1-dioxide; CNS, central nervous system; Cpd, compound; GluA2, AMPA receptor subunit 2; ITC, isothermal titration calorimetry; LBD, ligand-binding domain; MD, molecular dynamics; OSP, one-step perturbation; PEG, poly(ethylene glycol); RMS, root-mean-square; TI, thermodynamic integration; TMS, tetramethylsilane

■ REFERENCES

(1) Traynelis, S. F.; Wollmuth, L. P.; McBain, C. J.; Menniti, F. S.; Vance, K. M.; Ogden, K. K.; Hansen, K. B.; Yuan, H. J.; Myers, S. J.; Dingledine, R. Glutamate receptor ion channels: Structure, regulation, and function. *Pharmacol. Rev.* **2010**, *62*, 405−496.

(2) Sobolevsky, A. I.; Rosconi, M. P.; Gouaux, E. X-ray structure, symmetry and mechanism of an AMPA-subtype glutamate receptor. *Nature* **2009**, *462*, 745−756.

(3) Armstrong, N.; Gouaux, E. Mechanisms for activation and antagonism of an AMPA-sensitive glutamate receptor: Crystal structures of the GluR2 ligand binding core. *Neuron* **2000**, *28*, 165−181.

(4) Jin, R. S.; Clark, S.; Weeks, A. M.; Dudman, J. T.; Gouaux, E.; Partin, K. M. Mechanism of positive allosteric modulators acting on AMPA receptors. *J. Neurosci.* **2005**, *25*, 9027−9036.

(5) Sun, Y.; Olson, R.; Horning, M.; Armstrong, N.; Mayer, M.; Gouaux, E. Mechanism of glutamate receptor desensitization. *Nature* **2002**, *417*, 245−253.

(6) Leavit, S.; Freire, E. Direct measurement of protein binding energetics by isothermal titration calorimetry. *Curr. Opin. Struct. Biol.* **2001**, *11*, 560−566.

(7) Shirts, M. R.; Mobley, D. L.; Chodera, J. D. Alchemical free energy calculations: Ready for prime time? *Annu. Rep. Comp. Chem.* **2007**, *3*, 41−59.

(8) de Ruiter, A.; Oostenbrink, C. Free energy calculations of protein−ligand interactions. *Curr. Opin. Chem. Biol.* **2011**, *15*, 547−552.

(9) Reinhardt, W. P.; Miller, M. A.; Amon, L. M. Why is it so difficult to simulate entropies, free energies, and their differences. *Acc. Chem. Res.* **2001**, *34*, 607−614.

(10) Velazquez-Campoy, A.; Yoshiaki, K.; Freire, E. The binding energetics of first- and second-generation HIV-1 protease inhibitors: Implications for drug design. *Arch. Biochem. Biophys.* **2001**, *390*, 169−175.

(11) Lai, B.; Nagy, G.; Garate, J. A.; Oostenbrink, C. Entropic and enthalpic contributions to stereospecific ligand binding from enhanced sampling methods. *J. Chem. Inf. Model.* **2014**, *54*, 151−158.

(12) Reynolds, C. H.; Holloway, M. K. Thermodynamics of ligand binding and efficiency. *ACS Med. Chem. Lett.* **2011**, *2*, 433−437.

(13) Ben-Naim, A.; Marcus, Y. Solvation thermodynamics of nonionic solutes. *J. Chem. Phys.* **1984**, *81*, 2016−2027.

(14) van der Vegt, N. F. A.; van Gunsteren, W. F. Entropic contributions in co-solvent binding to hydrophobic solutes in water. *J. Phys. Chem. B* **2004**, *108*, 1056−1064.

(15) Lai, B.; Oostenbrink, C. Binding free energy, energy and entropy calculations using simple model systems. *Theor. Chem. Acc.* **2012**, *131*, 1272.

(16) Nørholm, A.-B.; Francotte, P.; Olsen, L.; Krintel, C.; Frydenvang, K.; Goffin, E.; Challal, S.; Danober, L.; Botez-Pop, I.; Lestage, P.; Pirotte, B.; Kastrup, J. S. Synthesis, pharmacological and structural characterization, and thermodynamic aspects of GluA2-positive allosteric modulators with a 3,4-dihydro-2H-1,2,4-benzothiadiazine 1,1-dioxide scaffold. *J. Med. Chem.* **2013**, *56*, 8736−8745.

(17) Beveridge, D. L.; DiCapua, F. M. Free energy via molecular simulation: Applications to Chemical and Biomolecular Systems. *Annu. Rev. Biophys. Biophys. Chem.* **1989**, *18*, 431−492.

(18) Oostenbrink, C. Free Energy Calculations from One-Step Perturbations. In *Methods in Molecular Biology, Computational Drug Discovery and Design*, Baron, R., Ed.; Humana Press: New York, 2012; Vol. *819*, pp 487−499.

(19) Francotte, P.; Goffin, E.; Fraikin, P.; Lestage, P.; Van Heugen, J. C.; Gillotin, F.; Danober, L.; Thomas, J. Y.; Chiap, P.; Caignard, D. H.; Pirotte, B.; de Tullio, P. New fluorinated 1,2,4-benzothiadiazine 1,1-dioxides: Discovery of an orally active cognitive enhancer acting through potentiation of the 2-amino-3-(3-hydroxy-5-methylisoxazol-4-yl) propionic acid receptors. *J. Med. Chem.* **2010**, *53*, 1700−1711.

(20) Francotte, P.; Goffin, E.; Fraikin, P.; Graindorge, E.; Lestage, P.; Danober, L.; Challal, S.; Rogez, N.; Nosjean, O.; Caignard, D. H.; Pirotte, B.; de Tullio, P. Development of thiophenic analogues of benzothiadiazine dioxides as new powerful potentiators of 2-amino-3-(3-hydroxy-5-methylisoxazol-4-yl)propionic acid (AMPA) receptors. *J. Med. Chem.* **2013**, *56*, 7838−7850.

(21) Lockhart, B.; Iop, F.; Closier, M.; Lestage, P. (S)-2,3-Dihydro-3,4 cyclopentano-1,2,4-benzothiadiazine-1,1-dioxide: (S18986-1) a positive modulator of AMPA receptors enhances (S)-AMPA-mediated H-3 noradrenaline release from rat hippocampal and frontal cortex slices. *Eur. J. Pharmacol.* **2000**, *401*, 145−153.

(22) Krintel, C.; Frydenvang, K.; Olsen, L.; Kristensen, M. T.; de Barrios, O.; Naur, P.; Francotte, P.; Pirotte, B.; Gajhede, M.; Kastrup, J. S. Thermodynamics and structural analysis of positive allosteric modulation of the ionotropic glutamate receptor GluA2. *Biochem. J.* **2012**, *441*, 173−178.

(23) Schmid, N.; Christ, C. D.; Christen, M.; Eichenberger, A. P.; van Gunsteren, W. F. Architecture, implementation and parallelisation of the GROMOS software for biomolecular simulation. *Comput. Phys. Commun.* **2012**, *183*, 890−903.

(24) Eichenberger, A. P.; Allison, J. R.; Dolenc, J.; Geerke, D.; Horta, B. A. C.; Meier, K.; Oostenbrink, C.; Schmid, N.; Steiner, D.; Wang, D.; van Gunsteren, W. F. GROMOS++ software for the analysis of biomolecular simulation trajectories. *J. Chem. Theor. Comp.* **2011**, *7*, 3379−3390.

(25) Reif, M. M.; Hünenberger, P. H.; Oostenbrink, C. New interaction parameters for charged amino acid side chains in the GROMOS force field. *J. Chem. Theor. Comp.* **2012**, *8*, 3705−3723.

(26) Zagrovic, B.; van Gunsteren, W. F. Computational analysis of the mechanism and thermodynamics of inhibition of phosphodiesterase 5A by synthetic ligands. *J. Chem. Theor. Comp.* **2007**, *3*, 301−311.

(27) Fioroni, M.; Burger, K.; Mark, A. E.; Roccatano, D. A new 2,2,2-trifluoroethanol model for molecular dynamics simulations. *J. Phys. Chem. B* **2000**, *104*, 12347−12354.

(28) Berendsen, H. J. C.; Postma, J. P. M.; van Gunsteren, W. F.; DiNola, A.; Haak, J. R. Molecular-dynamics with coupling to an external bath. *J. Chem. Phys.* **1984**, *81*, 3684−3690.

(29) Martyna, G.; Klein, M. L.; Tuckerman, M. Nosé-Hoover chains: The canonical ensemble via continuous dynamics. *J. Chem. Phys.* **1992**, *97*, 2635−2643.

(30) Koehler, J. E. H.; Saenger, W.; van Gunsteren, W. F. On the occurrence of three-centre hydrogen bonds in cyclodextrins in crystalline form and in aqueous solution: Comparison of neutron diffraction and molecular dynamics results. *J. Biomol. Struct. Dyn.* **1988**, *6*, 181−198.

(31) Kabsch, W.; Sander, C. Dictionary of protein secondary structure: Pattern recognition of hydrogen-bonded and geometrical features. *Biopolymers* **1983**, *22*, 2577−2637.

(32) Tembe, B. L.; McCammon, J. A. Ligand−receptor interactions. *Comput. Chem.* **1984**, *8*, 281−283.

(33) Riniker, S.; Christ, C. D.; Hansen, H. S.; Hünenberger, P. H.; Oostenbrink, C.; Steiner, D.; van Gunsteren, W. F. Calculation of relative free rnergies for ligand-protein binding, solvation and conformational transitions using the GROMOS software. *J. Phys. Chem. B* **2011**, *115*, 13570−13577.

(34) Beutler, T. C.; Mark, A. E.; van Schaik, R. C.; Gerber, P. R.; van Gunsteren, W. F. Avoiding singularities and numerical instabilities in free energy calculations based on molecular simulations. *Chem. Phys. Lett.* **1994**, *222*, 529−539.
(35) Kirkwood, J. G. Statistical mechanics of fluid mixtures. *J. Chem. Phys.* **1935**, *3*, 300−313.
(36) Torrie, G. M.; Valleau, J. P. Monte Carlo free energy estimates using non-Boltzmann sampling: Application to the sub-critical Lennard−Jones fluid. *Chem. Phys. Lett.* **1974**, *28*, 578−581.
(37) Torrie, G. M.; Valleau, J. P. Nonphysical sampling distibutions in Monte Carlo free-energy estimation: Umbrella sampling. *J. Comput. Phys.* **1977**, *23*, 187−199.
(38) Liu, H. Y.; Mark, A. E.; van Gunsteren, W. F. Estimating the relative free energy of different molecular states with respect to a single reference state. *J. Phys. Chem.* **1996**, *100*, 9485−9494.
(39) Schäfer, H.; van Gunsteren, W. F.; Mark, A. E. Estimating relative free energies from a single ensemble: Hydration free energies. *J. Comput. Chem.* **1999**, *20*, 1604−1617.
(40) Zwanzig, R. W. High-temperature equation of state by a perturbation method. I. Nonpolar gases. *J. Chem. Phys.* **1954**, *22*, 1420−1426.
(41) Peter, C.; Oostenbrink, C.; van Dorp, A.; van Gunsteren, W. F. Estimating entropies from molecular dynamics simulations. *J. Chem. Phys.* **2004**, *120*, 2652−2661.
(42) Meerwein, H.; Dittmar, G.; Gollner, R.; Hafner, K.; Mensch, F.; Steinfort, O. Untersuchungen uber aromatische diazoverbindungen 0.2. Verfahren zur herstellung aromatischer sulfonsaurechloride, eine neue modifikation der Sandmeyerschen reaktion. *Chem. Ber./Recl.* **1957**, *90*, 841−852.
(43) Francotte, P.; Nørholm, A.-B.; Deva, T.; Olsen, L.; Frydenvang, K.; Goffin, E.; Fraikin, P.; De Tullio, P.; Challal, S.; Thomas, J.-Y.; Iop, F.; Louis, C.; Botez-Pop, I.; Lestage, P.; Danober, L.; Kastrup, J.; Pirotte, B. Positive allosteric modulators of 2-amino-3-(3-hydroxy-5-methylisoxazol-4-yl)propionic acid (AMPA) receptors belonging to 4-cyclopropyl-3,4-dihydro-2H-1,2,4-pyridothiadiazine dioxides and diversely chloro-substituted 4-cyclopropyl-3,4-dihydro-2H-1,2,4-benzothiadiazine 1,1-dioxides. *J. Med. Chem.* **2014**, *57*, 9539−9553.
(44) Cowen, M. S.; Beart, P. M. Cyclothiazide and AMPA receptor desensitization: Analyses from studies of AMPA-induced release of H-3-noradrenaline from hippocampal slices. *Br. J. Pharmacol.* **1998**, *123*, 473−480.
(45) Shirts, M.; Mobley, D.; Brown, S. Free-Energy Calculations in Structure-Based Drug Design. In *Drug Design: Structure- and Ligand-Based Approaches*; Merz, K. M.; Ringe, D.; Reynolds, C.H., Eds.; Cambridge University Press: New York, 2010; pp 61−86.